J. Fluid Mech. (1989), *vol.* 207, *pp.* 379–392
Printed in Great Britain

Flow development in a model airway bronchus

By B. SNYDER[1] AND D. E. OLSON[2]

[1] Department of Mechanical Engineering, University of Nevada – Reno, Reno, NV 89557, USA
[2] Department of Mechanical Engineering, Wichita State University, Wichita, KS 67208, USA

(Received 17 August 1987 and in revised form 28 February 1989)

Three-dimensional laminar flow profiles were measured at each of three axial stations downstream from the inlet of a slowly tapering tube of constant flow cross-section. It was found that strong inlet wall shear induces significant secondary swirl, whose downstream growth is initially consistent with an inviscid model of vorticity transfer. This secondary flow may act to retard the onset of local flow separation by convecting axial momentum into the boundary layer adjacent to the diverging wall of the tube. These observations could account for the similar geometric shape of major bronchial airways: the suppression of flow separation in pulmonary bifurcations would promote more effective airway ventilation in the human lung.

1. Introduction

During breathing, inhaled air is transported through bronchial passages which recurrently branch to produce an enormous increase in flow cross-section: the total flow area of the many small terminal airways in the human lung is several hundred times that of the tracheal inlet. As flow separation would be certain to occur in a simple diffuser analogue of this system, it would be of interest to know if it can be avoided in the diverging airway system. Separation is likely to be deleterious to the normal function of the lung because it increases inspiratory head loss and creates favoured pathways, by which distal regions of the lung would be ventilated unequally.

Evidence that flow separation is either absent or at least ameliorated in large airways comes from two different kinds of data. Direct measurements of velocity profiles in casts of recurrently branching sections of the pulmonary airways yield flow patterns that are characterized by strong wall shears, relatively skewed central profiles and the absence of backflow (Sudlow, Olson & Schroter 1970). Indirect evidence comes by comparing inspiratory and expiratory pressure drops in central airway casts: resulting head loss is nearly independent of flow direction. By contrast, in simple recurrently branching models for which separation is prominent, head loss is highly dependent on flow direction (Snyder *et al.* 1987). Lighthill (1972) has suggested that the importance of preventing flow separation can be inferred from airway design: at first, flow area increases very gradually with airway generation, until local Reynolds numbers, Re, become low enough that the effects of separation would be minimal. To date, this remains the only known rationale which can account, at least in part, for the geometry of major airways.

Our hypothesis is that the mechanisms responsible for retarding flow separation in the conducting airways act primarily in the tapering bronchial segment upstream of each airway bifurcation (figure 1). Here, the upstream circular bronchus gradually deforms into a tube of progressively greater ellipticity, prior to bifurcating into two

daughter branches. In the model (figure 2) local separation would seem inevitably to occur at some point, as the diverging wall is extended indefinitely. However, streamline curvature associated with this geometric tapering forms secondary flows which could delay the onset of separation. In this manuscript we report on a variety of the flow patterns observed experimentally for a symmetric model of the tapering bronchial segment.

Similar models have been the subject of several recent physiological investigations. Gaver & Grotberg (1986) used a two-dimensional model of a bronchial segment to study the effect of oscillatory flow irreversibility on enhanced convective mixing. Their data show negligible frequency effects for values of the Womersley parameter $a_0(\omega/\nu)^{\frac{1}{2}} \leqslant 5$, suggesting that in normal breathing flow is quasi-steady throughout the bronchial tree. Bertram & Pedley (1983) studied incipient flow separation in a two-dimensional tapered channel which was indented along one side, and found that three-dimensional eddying motion was produced on the leeward side of the indentation. Wild, Pedley & Riley (1977) used lubrication theory to model transmural collapse induced by the viscous flow of blood through such a tube.

Apart from its potential importance to physiology, the evolution of secondary flows in a tapered segment is interesting in its own right, being one of the simplest cases for which the developing geometry of a conduit governs the evolution of flow. Using a perturbation method, Sobey (1976) found analytically that flow patterns resulting from an axisymmetric inlet profile should initially remain matched to wall geometry, and therefore acquire an elliptical symmetry. Downstream, however, streamline curvature induces significant secondary flows, which must ultimately vanish as the flow approaches the swirl-free, Poiseuille limit. Precisely this quality of transience makes the model significant to our general understanding of developing flows.

2. Methods

The flow model used in these experiments was designed to simulate in a simplified way the transition zone adjacent to the flow divider in airway bifurcations, as illustrated in figure 1. Consequently, its inlet cross-section was circular, which then gradually deformed downstream into elliptical cross-sections of progressively greater eccentricity. The rate of tapering was similar to that of airways, but the test section extended somewhat beyond the point at which the 'typical' bronchial segment bifurcates. Since bronchial segments in the major airways exhibit a wide range of aspect (length/diameter) ratios, an extended length permits wider inferences to be drawn with regard to their role in conditioning airway flow.

Figure 2 shows geometric details of the model, illustrating the development of the flow lumen at successive stages downstream. The geometry of the test section is specified by two independent parameters – the inlet radius a_0 and the wall radius of curvature R, in the plane of the major semi-axis. At an axial distance Z downstream from the inlet, the cross-sectional shape is given by $X^2/a^2 + Y^2/b^2 = 1$, with $a(Z)$ and $b(Z)$ the major and minor semi-axes respectively. At this distance the major semi-axis is determined by the curvature of the outer wall, so that $a(Z) = a_0 + R - (R^2 - Z^2)^{\frac{1}{2}}$. The minor semi-axis correspondingly decreases, so as to maintain the cross-sectional area constant. The wall curvature ratio $R/a_0 = 24/2.54 \approx 9.5$ is equivalent to a tightly coiled pipe bend, so that streamline curvature was expected to produce significant downstream swirl.

A fibreglass model of the test section was cast from a mould in half-sections, its

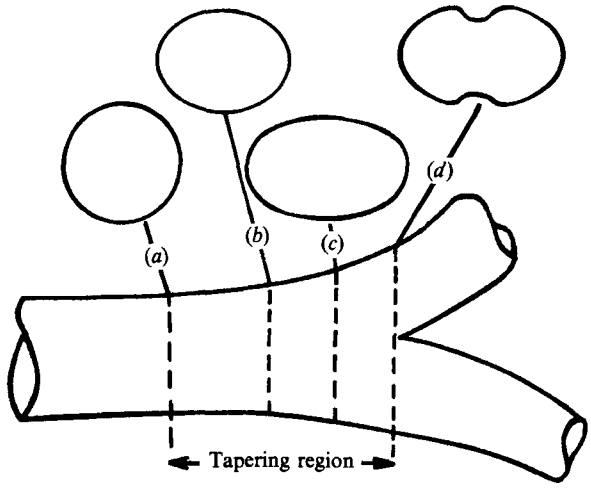

FIGURE 1. Flow geometry of a typical bronchial segment, as described by Horsfield *et al.* (1971). Prior to bifurcating into downstream segments, the upstream circular cross-section tapers into an elliptical segment of nearly the same cross-sectional area (*b*). This shape then flattens (*c*) as its minor axis approximates to the diameter of the daughter branches (*d*), while its area increases. The total distance between successive bifurcation points varies widely, but commonly is 3.5 bronchial diameters; the tapering region extends less than two diameters.

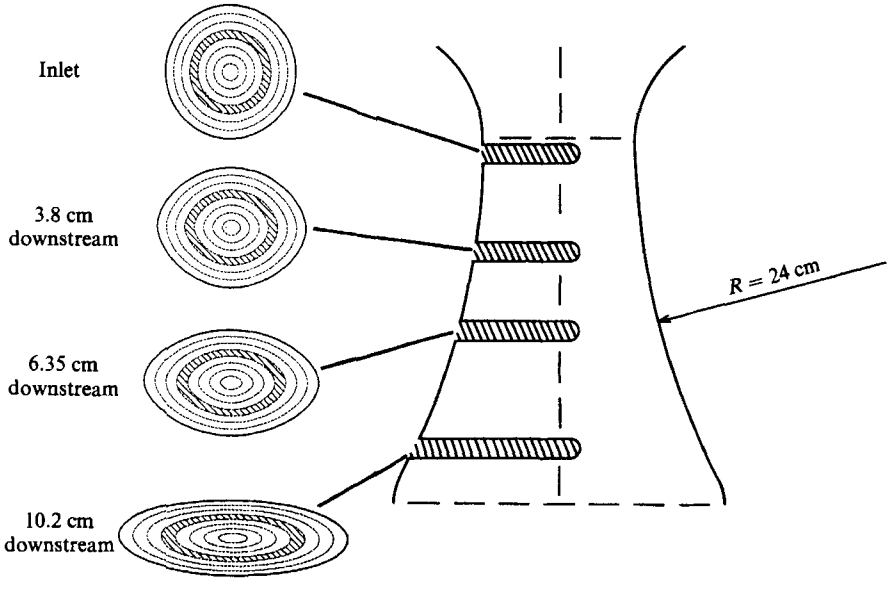

FIGURE 2. Flow geometry of the test section, showing the placement of hot-wire slots downstream from the circular inlet. Corresponding elliptical cross-sections are shown subdivided into concentric rings, within each of which (shaded area) partial flow is found to be conserved. Flow area is constant throughout the tapering segment, corresponding to cases (*a*) and (*b*) of figure 1. Wall radius of curvature is 24 cm; inlet diameter, 5.1 cm; resulting wall curvature ratio is similar to (*a*–*d*) of figure 1.

walls polished, then assembled. Slots were milled into its walls at four axial positions to permit access by a flow probe. This sensor, a parallel-wire pulsed-probe anemometer, determines both the local fluid velocity and its flow direction by measuring the time of flight and axial wake of a thermal cloud, generated at an upstream pulse wire and detected at a downstream sensor wire (Olson, Parker & Snyder 1984). A rotameter located upstream of the inlet flow plenum was used to monitor flow rate. Flow entering the plenum was screened and straightened, then passed through an entrance bell to obtain a swirl-free, flat inlet profile. This profile was checked by hot-wire measurements taken along the horizontal and vertical axes of the inlet cross-section to define the extent of the wall vortex ring. Parabolic inlet cases were generated by interposing a straight, thermally insulated pipe 100 dia. in length between the entrance bell and the test section. In additional cases, a 90° curved-pipe section (curvature ratio $R/a = 3.5$) was used to generate skewed, swirling inlet profiles that are more typical of flow patterns in pulmonary airways.

Based on airway dimensions and physiological flow rates, the characteristic Reynolds numbers in large airways are of the order of several hundred (Horsfield *et al.* 1971). However, Re is unlikely to be an appropriate scaling parameter for dynamic similarity in this case. Using $L/D \approx 0.06Re$ as a crude estimate of entrance length indicates that the test section, with an overall $L/D = 2$, is too short to permit any significant development of viscous effects at prototypical Re. Therefore in selecting flow parameters we assumed that flow development would be nearly inviscid, laminar, and kinematically similar to corresponding airway flows.

3. Results

The primary data comprise axial (Z-) and transverse (X-, Y-) velocity components, measured at 2 mm intervals along four horizontal and either four or five vertical traverses spaced equally throughout each flow cross-section. Two different flow rates were used to determine any effect of Reynolds number $\overline{W}D/\nu$ ($\overline{W}$ = mean axial velocity, D = inlet diameter; ν = kinematic viscosity of air). From these data, isovelocity contours were constructed to illustrate the evolution of the axial velocity profile at entrance lengths 3.8 cm (1.5 in.), 6.35 cm (2.5 in.) and 10.2 cm (4 in.) downstream from the circular inlet. Examples of isovelocity contours resulting from a flat inlet profile have been reported previously (Snyder & Olson 1986); those from a parabolic profile are shown in figure 3. Both Re values show a consistent pattern of development, although distributions at low Re are more peaked owing to the greater difficulty in maintaining the inlet profile parabolic.

Both flat and parabolic inlet cases develop in a similar manner. Near the inlet, isovelocity contours conform to the geometric boundaries, becoming progressively compressed along the minor axis while expanding along the major axis. Further downstream, however, flow patterns do not remain elliptically symmetric in either case. The magnitude of axial velocities on any given concentric ellipse typically varies at least two-fold except near the central core, being minimal on the major axis and maximal on the minor axis. Figure 3 makes evident the progressive dissociation of the flow contour from the wall boundary. Thus flow begins to lag the conduit geometry, which makes plausible that in the absence of secondary currents separation might eventually occur along the diverging wall of the tube. In fact, however, no region of separation was actually observed under any inlet condition.

The development of flow lag coincides with the onset of transverse secondary currents. To understand why, it is useful to consider the simple qualitative model

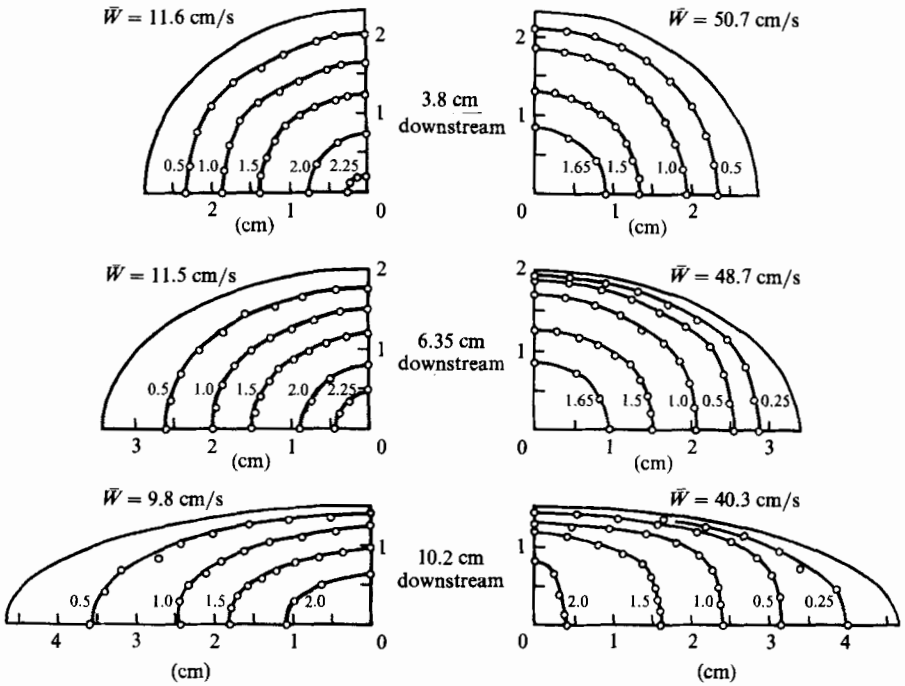

FIGURE 3. Axial isovelocity contours in the entrance region of the elliptical segment; parabolic inlet profile. Each contour is normalized by the mean axial velocity $\bar{W}$. Left-hand panels: Reynolds number $\approx$ 380. Right-hand panels: Reynolds number $\approx$ 1540.

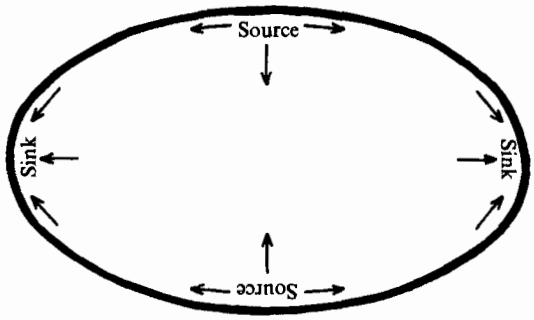

FIGURE 4. Model for formation of secondary currents. The converging wall adjacent the minor semi-axis acts as a flow source, while that of the diverging major semi-axis acts as a sink. As a consequence currents should not form closed streamlines, but instead convect a continuous supply of momentum to the diverging wall.

shown in figure 4. Evidently the converging walls of the tube act locally to produce flow sources, while the diverging walls generate sinks. The resulting secondary motions form a net convective current, leaving the converging wall and directed towards the diverging wall in each quadrant of the flow section. This flow pattern is distinct, therefore, from the closed streamline motion of Dean-type vortices associated with fully developed flow in a uniformly curved pipe. Its currents can be expected to supply a continuous source of momentum to the diverging wall, which has important implications for boundary-layer development, as discussed later in this report. In addition, the model indicates that the experimental outcome is likely

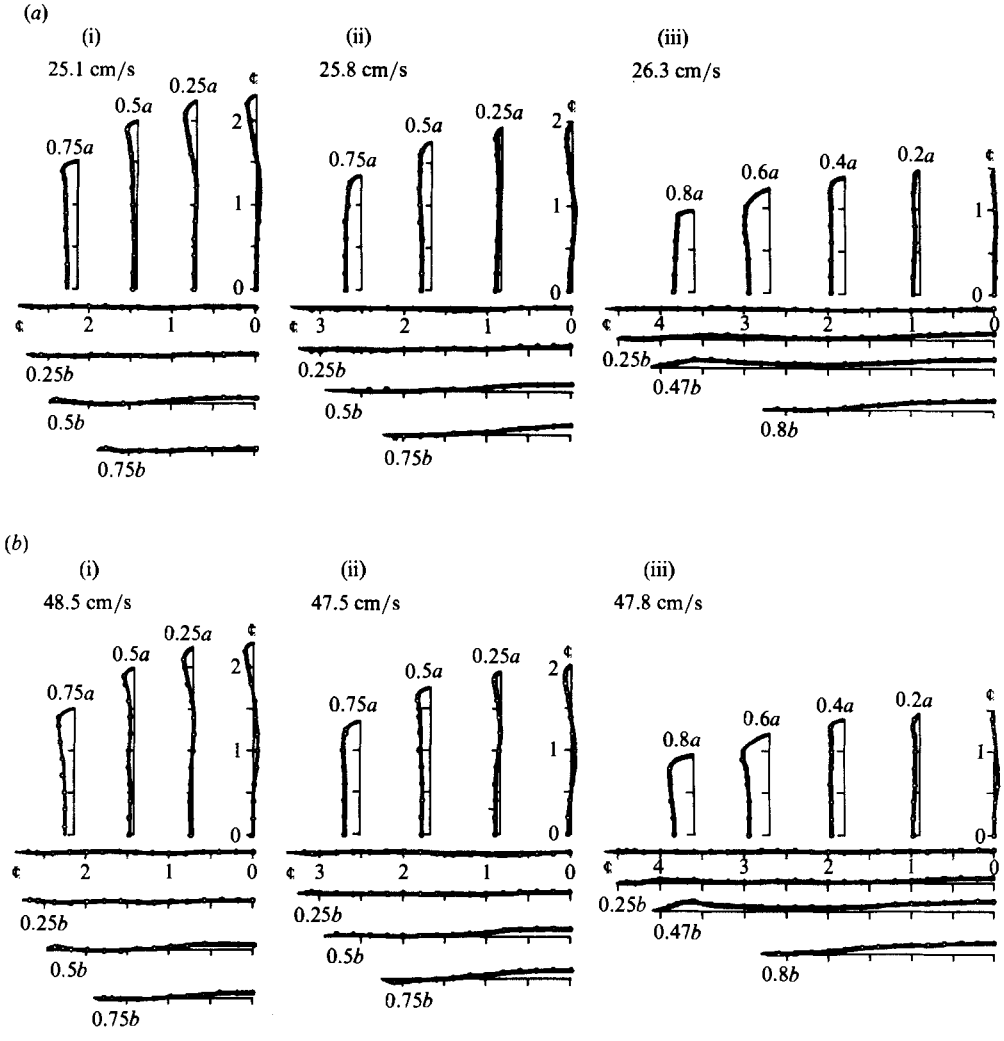

FIGURE 5(*a*, *b*). For caption see facing page.

to underestimate the swirl intensity in the prototypical bronchial segment of figure 1: its indented margins, in (*d*), can be expected to amplify the flow sources which initiate the currents.

Transverse X- and Y-components of velocity, measured at the three downstream stations of the flow section, are shown in figure 5(*a*, *b*, *c*) for both inlet conditions. (Data for the parabolic inlet are less complete, as the corrections needed to account for natural convection at low Re proved too large to yield reliable information.) A few minor peculiarities which recur at successive downstream stations are probably attributable to small defects in the inlet flow profiles. However, the overall flow patterns confirm the basic physical model outlined above. Both Re sequences generated by the flat inlet profile, in figure 5(*a*, *b*), are kinematically similar at each stage in almost every detail. This provides substantiation that entrance flow in a tapering section can be understood in terms of an *inviscid* model. The parabolic case, in figure 5(*c*), differs somewhat in details of its development. Swirl in the boundary layer appears to be less intense, consistent with the weaker wall shear present at the

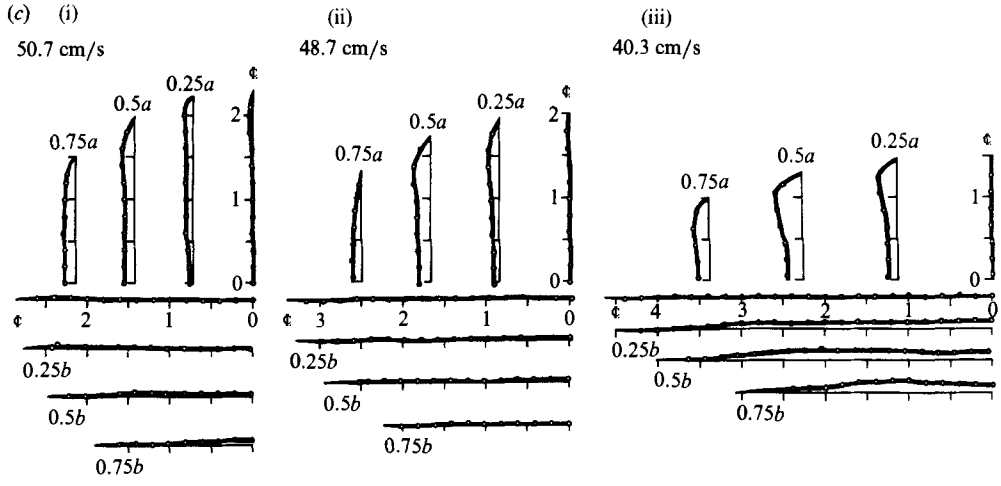

FIGURE 5. Transverse velocity profiles, showing the downstream evolution from swirl-free inlet flow. (*a*) Uniform inlet, $Re = 840$; (*b*) uniform inlet, $Re = 1560$; (*c*) parabolic inlet, $Re = 1540$. (i) $Z = 3.8$ cm downstream; (ii) $Z = 6.35$ cm; (iii) $Z = 10.2$ cm. Velocities are scaled so that $0.2\bar{W}$ corresponds to 0.5 cm on interval markers. Vertical components are displaced from the upper quadrant of the flow section; positive values signify flow towards the centreline. Locations of traverses are normalized to major semi-axis (a) or minor semi-axis (b).

inlet. Conversely, near the centreline the secondary flows are somewhat greater for the parabolic case. These second-order differences are predicted by a quantitative model for the development of secondary vorticity, as discussed below.

4. Discussion

Sobey (1976) formulated a systematic perturbation method to account for inviscid secondary flows produced in a tapering elliptical tube. Utilizing this procedure, he obtained expressions for the downstream secondary velocity and vorticity components resulting from a small axisymmetric shear δ in the inlet velocity profile. His predicted distribution of secondary axial velocity at a distance Z downstream from the inlet is

$$[U_0\delta^2]\left[A(Z)\left(\frac{Y^2}{b^2}-\frac{X^2}{a^2}\right)+B(Z)\left(\frac{Y^4}{b^4}-\frac{X^4}{b^4}\right)\right],$$

where $A(Z)$ and $B(Z)$ are complicated functions of tube geometry. This expression predicts that the secondary flow integrated along any interior ellipse concentric to the boundary should be zero. It can be tested by subdividing each of the flow cross-sections into concentric elliptical areas, as represented in figure 2, then computing the partial flow through each ellipse using the experimental data of figure 3. Each partial flow should remain constant as flow proceeds downstream and as its flow ring becomes progressively more eccentric. The calculations summarized in table 1 for the parabolic cases indicate that this condition is nearly fulfilled: the greatest discrepancy occurs for the inlet distributions (for which data were available only along the major and minor axes), as compared to the more complete downstream cases. The corresponding results for the flat inlet cases show a similar degree of flow invariance (Snyder & Olson 1986). Thus by inference, convective mixing is promoted within rather than between rings. We feel that these results represent strong

Ring no.	Inlet	3.8 cm	6.35 cm	10.2 cm	Average ± SD†
			$Re = 380$		
1	0.0327	0.0369	0.0365	0.0389	0.0374 ± 0.0013
2	0.0931	0.1038	0.1040	0.1074	0.1051 ± 0.0020
3	0.1419	0.1547	0.1568	0.1557	0.1557 ± 0.0011
4	0.1732	0.1836	0.1869	0.1799	0.1835 ± 0.0037
5	0.1842	0.1860	0.1878	0.1799	0.1846 ± 0.0041
6	0.1752	0.1629	0.1609	0.1594	0.1611 ± 0.0018
7	0.1401	0.1214	0.1181	0.1243	0.1213 ± 0.0031
8	0.0596	0.0506	0.0490	0.0544	0.0513 ± 0.0028
			$Re = 1540$		
1	0.0283	0.0286	0.0272	0.0326	0.0295 ± 0.0028
2	0.0835	0.0835	0.0812	0.0911	0.0853 ± 0.0052
3	0.1345	0.1329	0.1324	0.1380	0.1344 ± 0.0031
4	0.1761	0.1725	0.1748	0.1714	0.1729 ± 0.0017
5	0.1966	0.1937	0.1972	0.1869	0.1926 ± 0.0052
6	0.1849	0.1856	0.1879	0.1762	0.1832 ± 0.0062
7	0.1396	0.1437	0.1421	0.1414	0.1424 ± 0.0012
8	0.0565	0.0596	0.0573	0.0624	0.0598 ± 0.0026

† Average and standard deviation of three downstream measurements.

TABLE 1. Distribution of partial flows in the entry region of the elliptical test section, parabolic inlet profile

evidence for the essential appropriateness of this inviscid model, as applied for moderate Reynolds numbers.

We were equally interested in testing Sobey's expression for the secondary axial vorticity ω_z, resulting from the interaction of δ with streamline curvature:

$$\omega_z \propto c(Z)\,\delta. \tag{1}$$

This expression indicates qualitatively why a uniform inlet profile, with relatively greater shear δ near the walls, should induce stronger boundary-layer currents than does a parabolic profile. In addition, the c-parameter $c(Z)$ provides a 'natural' lengthscale for secondary flow development, and for the case of constant flow cross-section is given by

$$c(Z) = \int_{-\infty}^{Z} \left\{ a^2 \frac{\mathrm{d}}{\mathrm{d}s}\left[\frac{\mathrm{d}a/\mathrm{d}s}{a}\right] - b^2 \frac{\mathrm{d}}{\mathrm{d}s}\left[\frac{\mathrm{d}b/\mathrm{d}s}{b}\right] \right\} \mathrm{d}s. \tag{2}$$

By interpreting the lower limit $(-\infty)$ as signifying the inlet $(Z \leqslant 0)$ where streamline curvature is zero, $c(Z)$ can be evaluated numerically from (2). The particular computed curve appropriate to our test section is graphed as a solid line in each of the figures 6(a) and 6(b). Far downstream, this curve can be seen to approach a limiting maximum value.

In general, an exact comparison of $c(Z)$ with experimental values of secondary vorticity is difficult, because ω_z in (1) should be dependent on the transverse spatial coordinates X and Y. This can be verified by considering Sobey's equation (24a):

$$\omega_z = \frac{-2\epsilon\delta}{s}\left(Y_0 \frac{\partial t_1}{\partial x_0} - X_0 \frac{\partial t_1}{\partial Y_0} \right) + O(\delta^2).$$

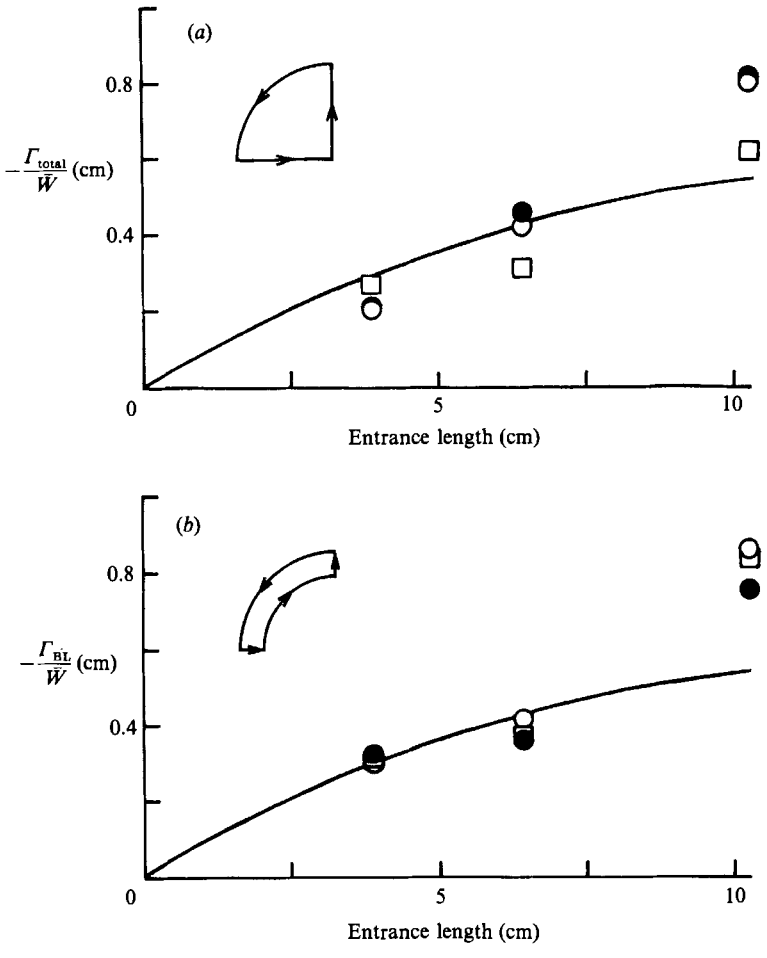

FIGURE 6. (*a*) Evolution of total circulation Γ_{total} (see inset) for ●, ○, flat and □, parabolic inlet profiles. The corresponding relative growth of the c-parameter (defined by (2)) is indicated by solid line. (*b*) Comparable evolution of boundary-layer circulation Γ_{BL}, defined in inset. Circulation loops enclose approximately 20% of total quadrant.

Here the subscript '0' refers to the inlet, ϵ is a small length parameter, s is the flow cross-section (which is constant in our case), and t_1 is that portion of Lighthill's t-parameter which depends on X_0 and Y_0:

$$t_1(Z, X_0, Y_0) = \frac{-1}{2}\left\{Y_0^2 \int_{-\infty}^{Z} a^2 \frac{\mathrm{d}}{\mathrm{d}s}\left(\frac{\mathrm{d}a/\mathrm{d}s}{a}\right)\mathrm{d}s + X_0^2 \int_{-\infty}^{Z} b^2 \frac{\mathrm{d}}{\mathrm{d}s}\left(\frac{\mathrm{d}b/\mathrm{d}s}{b}\right)\right\}\mathrm{d}s.$$

Carrying out the differentiation,

$$\omega_z \propto X_0 Y_0 c(Z)\,\delta.$$

Since ω_z induced on a streamline originating at (X_0, Y_0) is associated permanently with that particular streamline, it therefore depends on downstream spatial location (X, Y).

Using Stokes' theorem,

$$\int \omega_z \,\mathrm{d}X\,\mathrm{d}Y = \oint \boldsymbol{V}\cdot\boldsymbol{dl} = \Gamma,$$

to relate experimental values of circulation, Γ, to the predicted ω_z requires knowledge of the downstream spatial evolution of individual streamlines. Matters can be greatly simplified by taking Γ_{total} over an entire quadrant of the cross-section, bounded by the two axes of symmetry. As the flow cross-section remains constant through each downstream station, the numerical value of the area factor relating Γ_{total} to ω_z is immaterial: in any case, the length parameter ϵ is undefined. Moreover, the shear δ is relatively insensitive to the shape of the inlet flow profile, when averaged over a flow quadrant. The area-weighted δ for a parabolic profile is $-5.33\overline{W}/D$; δ for a uniform profile is $-(4.5\pm0.1)\,\overline{W}/D$ for boundary-layer thicknesses typical of these experiments, which ranged between 20–30% of the inlet diameter D.

Therefore both inlet cases are included in figure 6(*a*), which compares the growth of Γ_{total} evaluated from the experimental data with $c(Z)$ as numerically evaluated from (2). The c-parameter has been scaled to fit the data at the first two downstream stations; deviations from theory at the far-downstream point are consistent but too small to be conclusive.

Somewhat similar results were obtained by evaluating the circulation Γ_{BL} produced by the boundary-layer currents. Paths were chosen to maximize circulation while maintaining the enclosed loop areas equal through successive axial stages. (Loop areas for the parabolic case needed to be consistently greater to obtain maximal values.) Since the boundary-layer currents are significantly greater than secondary flows in the core, values of Γ_{BL} are probably more accurate than Γ_{total}. This is certainly true for the parabolic inlet, for which computed Γ_{BL} are systematically larger than corresponding Γ_{total}. Γ_{total} is probably too small, owing to the flattened shape of the inlet profile (seen in figure 7). In the uniform-inlet cases Γ_{BL} usually falls within 10–20% of Γ_{total}, consistent with a nearly irrotational core with secondary vorticity concentrated near the wall. Figure 6(*b*) shows that, for each inlet condition, circulation continues to increase farther downstream than is predicted by theory. Though limited in accuracy, the available experimental results in figure 6(*a*, *b*) suggest that the c-parameter eventually begins to underpredict the strength of downstream axial vorticity.

The far-downstream field therefore requires an extension of Sobey's second-order method, as tertiary fluid motions become increasingly important. It would be useful to evaluate such motions, for the continuing development of transverse currents provides a means by which flow separation may be suppressed. The swirl currents convect axial momentum into the boundary layer adjacent to the diverging major semi-axis, and this added momentum could act to stabilize the boundary layer against the onset of flow separation. The absence of experimentally observed flow separation in the present study, discussed below, suggests that the wall currents increase rapidly enough to compensate for the locally destabilizing effect of the diverging wall. By contrast, the theoretical profile seems to develop an inflection point midway through the test section.

Any experimental indications of flow separation should have been evident from figure 7, which depicts the developing axial velocity profile along the major semi-axis. The upper panels illustrate that the wall shear for a flat inlet profile, while initially steep, gradually diminishes to a parabolic distribution. The lower panels show that an inlet parabolic profile subsides even more dramatically, resulting in the formation of an inflection point midway through the test section. In an inviscid fluid, Fjørtoft's theorem marks this point as likely to signal the onset of flow instability. The absence of any such instability might be due to viscosity, which is currently thought to inhibit the growth of instability in low laminar shear flows (Orszag &

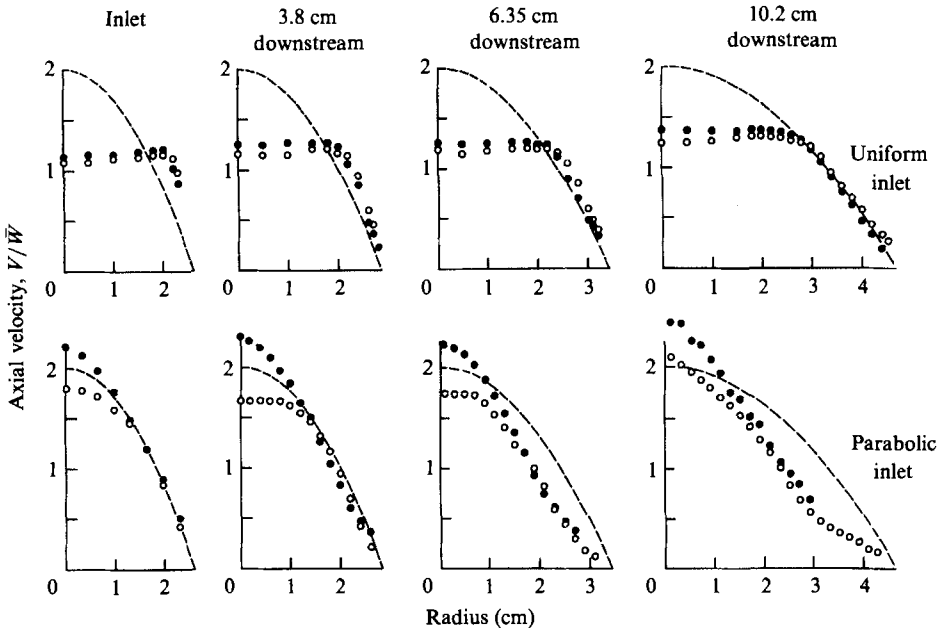

FIGURE 7. The downstream evolution of inlet flat and parabolic axial velocity profiles along the diverging major semi-axis: ●, low-*Re* cases; ○, high-*Re* cases. Dashed line shows for reference a parabolic velocity profile. The formation of an inflection point is evident in the lower panels.

Patera 1983). Since viscosity otherwise plays so limited a role in this test section – low- and high-*Re* velocity profiles being nearly superimposable – it seemed possible that flow separation might occur if the inlet shear were significantly weaker than in the parabolic case. Comparing the evolution of the two inlet profiles in figure 7, it appeared to us that separation in pulmonary airways might be retarded by the continual production of steep wall gradients (and consequently, intense swirl) on the flow dividers in the repeatedly branching flow stream. If this were so, then one key to flow stability in the airways lies in the recurrent nature of airway geometry itself.

To test this hypothesis, our investigation was extended to consider inlet profiles more typical of pulmonary airways, which exhibit pronounced skew and strong swirling currents (Pedley 1977). It was convenient to generate such flow patterns by interposing a uniformly curved 90°-bend between the entrance bell and the test section. A conventional hot-wire probe was used to record the evolution of velocity profiles along the major semi-axis of the tapering section. The measured signals were quite steady for inlet $Re \leqslant 1500$, but above this value, exhibited a low-frequency (≈ 13 Hz) oscillating component. Since these fluctuations were equally apparent at the inlet as well as downstream, they probably originated in the upstream curved-pipe segment, rather than in the test section. Therefore the high-*Re* cases were taken at a somewhat reduced flow velocity (43 cm/s) corresponding to a regime just below the onset of the instability.

The tightly coiled pipe ($R/a = 3.5$) produces the symmetrically peaked pattern seen in figure 8(*a*) when its symmetry plane is aligned perpendicular to the major semi-axis of the test section. Minor defects in the inlet profile become somewhat magnified downstream, producing a curiously asymmetric pattern of peaking midway through the section. Overall there is a clear-cut migration of the axial peak velocities outward towards the wall of the test section. No flow separation was seen

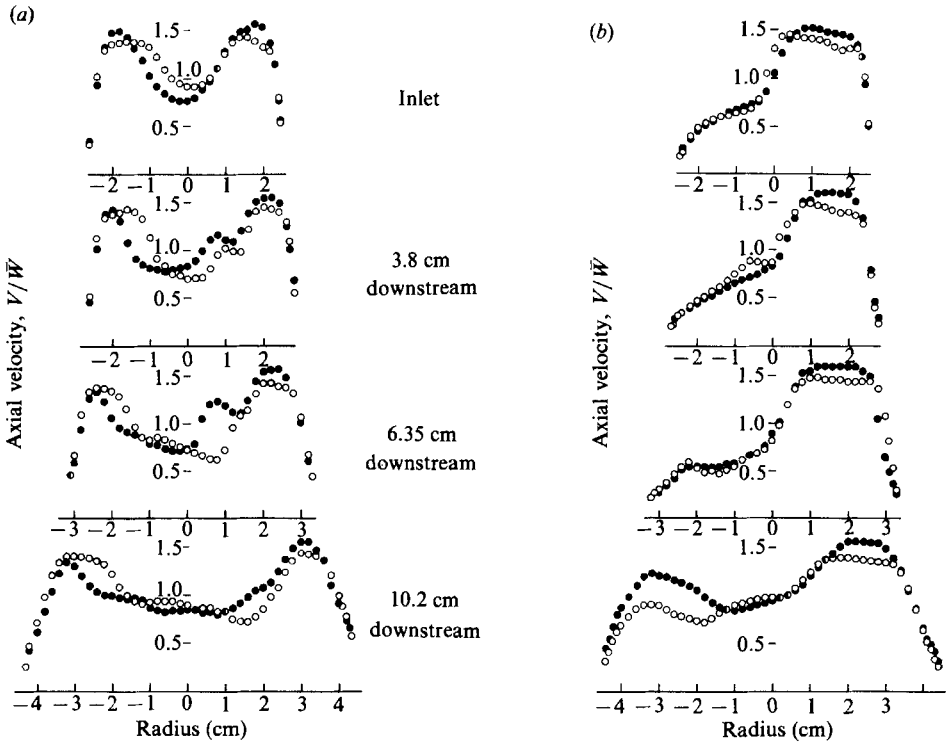

FIGURE 8. The evolution of prototypical skewed inlet profiles generated by a 90° pipe bend. Case (*a*) results when the symmetry plane of the bend is arranged perpendicular to the major semi-axis of the test section; case (*b*), when the symmetry plane is parallel. In neither case is flow separation observed.

or expected as the inlet gradient is weak only along the *converging* wall of the test section, and thus the flow is stabilized against the development of an inflection point.

Flow separation would seem more likely to occur if the symmetry plane of the pipe bend were aligned parallel to the major semi-axis. Successive panels of figure 8(*b*) show that at first the strong axial skew does remain confined along one wall, while the velocity gradient along the opposite wall becomes progressively weaker. Unexpectedly, however, this gradient then begins to steepen as flow progresses downstream, until development culminates in a pronounced double-peaked profile. Resulting downstream flow distributions are clearly 'advantageous' in two respects: shear is lowered as flow impinges onto the flow divider, and the flow itself is more equally distributed between the two daughter bifurcations.

This outcome suggests that the non-planar arrangement of airway architecture could itself aid in suppressing flow separation. A preliminary indication of its potential importance has been observed by J. R. Hammersley (private communication), who utilized hot-wire anemometry to measure local laminar velocity profiles in a multigeneration, symmetric, *planar* branching network. Although his model incorporated tapering bronchial segments and anatomically accurate branching ratios (to ensure a gradual reduction of *Re* through the system), the formation of inflection points and localized flow separation were observed at several regions within the network. As a consequence, exit flow distributions were highly non-uniform.

From the preliminary results presented in figure 8(*a*, *b*), it appears possible that airway flow patterns may be conditioned and restructured by bronchial segments to *anticipate* the presence of a downstream bifurcation. The distortion of the axial profile produces high velocities in the very regions where flow separation might occur as one progresses into the daughter branches and the mean flow velocity falls. Therefore, it would be useful to undertake a fully analysis of flow development in a tapering section. How inlet swirl interacts with axial skew to produce the development seen in figure 8(*b*) lies outside the scope of the present report.

5. Conclusions

Swirling currents form in a tapering elliptical flow segment as a result of the convection of inlet wall shear along curved streamlines; stream curvature itself is a consequence of the geometry. An inviscid second-order perturbation model predicts some aspects of the experimentally observed secondary flows rather well and is likely to be applicable to a wide category of converging–diverging flows. It does not account, however, for the continued growth of axial vorticity or the persistent stability of the flow profile adjacent the diverging tube wall. A more complete model needs to be formulated before we can begin to appreciate the reasons for the wide range of aspect ratios that characterize the geometry of major pulmonary airways.

Identifying the role of this flow segment is of fundamental importance to our understanding of pulmonary airflow. The data reported here indicate that inspiratory flow entering a bifurcation, where an area expansion occurs, may be conditioned against flow separation by the secondary flows produced in the upstream segment. The non-planar arrangement of airway architecture may itself aid in the suppression of flow separation: steep velocity gradients are recurrently formed at the bronchial walls by flow dividers; these gradients in turn produce secondary flows which inject momentum into the boundary layers. Data derived from more prototypical inlet flow patterns suggest that this segment may favourably condition entrance flow even under seemingly adverse inlet conditions.

B. Snyder wishes to thank the Whitaker Foundation for financial support provided throughout the duration of this investigation.

REFERENCES

Bertram, C. D. & Pedley, T. J. 1983 Steady and unsteady separation in an approximately two-dimensional indented channel. *J. Fluid Mech.* **130**, 315–345.

Gaver, D. P. & Grotberg, J. B. 1986 An experimental investigation of oscillatory flow in a tapered channel. *J. Fluid Mech.* **172**, 47–61.

Horsfield, K., Dart, G., Olson, D. E., Filley, G. F. & Cumming, G. 1971 Models of the human bronchial tree. *J. Appl. Physiol.* **31**, 207–217.

Lighthill, M. J. 1972 Physiological fluid dynamics: a survey. *J. Fluid Mech.* **52**, 475–497.

Olson, D. E., Parker, K. H. & Snyder, B. 1984 A pulsed wire probe for the measurement of velocity and flow direction in slowly moving air. *Trans. ASME* K: *J. Biomech. Engng* **106**, 72–78.

Orszag, S. A. & Patera, A. T. 1983 Hydrodynamic stability of shear flows. In *Les Houches*, Session XXXVI, 1981 (ed. G. Iooss, R. H. G. Hellman & R. Stora), pp. 623–662. North-Holland.

Pedley, T. J. 1977 Pulmonary fluid dynamics. *Ann. Rev. Fluid Mech.* **9**, 229–274.

Snyder, B. & Olson, D. E. 1986 Entrance-flow invariance in a tapering elliptical slit (letter). *Phys. Fluids* **29**, 2341–2343.

SNYDER, B., OLSON, D. E., HAMMERSLEY, J. R., PETERSON, C. V. & JAEGER, M. J. 1987 Reversible and irreversible components of central-airway flow resistance. *Trans. ASME* K : *J. Biomech. Engng* **109**, 154–159.

SOBEY, I. J. 1976 Inviscid secondary motions in a tube of slowly varying ellipticity. *J. Fluid Mech.* **73**, 621–639.

SUDLOW, M. F., OLSON, D. E. & SCHROTER, R. C. 1970 Fluid mechanics of bronchial air flow. In *Proc. 3rd Intl Congr. Inhaled Particles*, pp. 19–31. Allen and Unwin.

WILD, R., PEDLEY, T. J. & RILEY, D. S. 1977 Viscous flow in collapsible tubes of slowly varying elliptical cross-section. *J. Fluid Mech.* **81**, 273–294.